

SANDIA REPORT

SAND2014-0829
Unlimited Release
Printed March 2014

Sensitivity of Precipitation to Parameter Values in the Community Atmosphere Model Version 5

Gardar Johannesson, Donald Lucas, Yun Qian, Laura P. Swiler, and Timothy M. Wildey

Prepared by
Sandia National Laboratories
Albuquerque, New Mexico 87185 and Livermore, California 94550

Sandia National Laboratories is a multi-program laboratory managed and operated by Sandia Corporation, a wholly owned subsidiary of Lockheed Martin Corporation, for the U.S. Department of Energy's National Nuclear Security Administration under contract DE-AC04-94AL85000.

Approved for public release; further dissemination unlimited.



Sandia National Laboratories

Issued by Sandia National Laboratories, operated for the United States Department of Energy by Sandia Corporation.

NOTICE: This report was prepared as an account of work sponsored by an agency of the United States Government. Neither the United States Government, nor any agency thereof, nor any of their employees, nor any of their contractors, subcontractors, or their employees, make any warranty, express or implied, or assume any legal liability or responsibility for the accuracy, completeness, or usefulness of any information, apparatus, product, or process disclosed, or represent that its use would not infringe privately owned rights. Reference herein to any specific commercial product, process, or service by trade name, trademark, manufacturer, or otherwise, does not necessarily constitute or imply its endorsement, recommendation, or favoring by the United States Government, any agency thereof, or any of their contractors or subcontractors. The views and opinions expressed herein do not necessarily state or reflect those of the United States Government, any agency thereof, or any of their contractors.

Printed in the United States of America. This report has been reproduced directly from the best available copy.

Available to DOE and DOE contractors from
U.S. Department of Energy
Office of Scientific and Technical Information
P.O. Box 62
Oak Ridge, TN 37831

Telephone: (865) 576-8401
Facsimile: (865) 576-5728
E-Mail: reports@adonis.osti.gov
Online ordering: <http://www.osti.gov/bridge>

Available to the public from
U.S. Department of Commerce
National Technical Information Service
5285 Port Royal Rd
Springfield, VA 22161

Telephone: (800) 553-6847
Facsimile: (703) 605-6900
E-Mail: orders@ntis.fedworld.gov
Online ordering: <http://www.ntis.gov/help/ordermethods.asp?loc=7-4-0#online>



Sensitivity of Precipitation to Parameter Values in the Community Atmosphere Model Version 5

Gardar Johannesson
Lawrence Livermore National Laboratory
Livermore, CA 94551
johannesson1@llnl.gov

Donald Lucas
Lawrence Livermore National Laboratory
Livermore, CA 94551
lucas26@llnl.gov

Yun Qian
Pacific Northwest National Laboratory
P.O. Box 999
Richland, WA 99352
Yun.Qian@pnl.gov

Laura P. Swiler
Optimization and Uncertainty Quant.
Sandia National Laboratories
P.O. Box 5800
Albuquerque, NM 87185-1318
lpswile@sandia.gov

Timothy M. Wildey
Optimization and Uncertainty Quant.
Sandia National Laboratories
P.O. Box 5800
Albuquerque, NM 87185-1318
tmwilde@sandia.gov

Abstract

One objective of the Climate Science for a Sustainable Energy Future (CSSEF) program is to develop the capability to thoroughly test and understand the uncertainties in the overall climate model and its components as they are being developed. The focus on uncertainties involves sensitivity analysis: the capability to determine which input parameters have a major influence on the output responses of interest. This report presents some initial sensitivity analysis results performed by Lawrence Livermore National Laboratory (LNNL), Sandia National Laboratories (SNL), and Pacific Northwest National Laboratory (PNNL). In the 2011-2012 timeframe, these laboratories worked in collaboration to perform sensitivity analyses of a set of CAM5, 2° runs, where the response metrics of interest were precipitation metrics. The three labs performed their sensitivity analysis (SA) studies separately and then compared results. Overall, the results were quite consistent with each other although the methods used were different. This exercise provided a robustness check of the global sensitivity analysis metrics and identified some strongly influential parameters.

Acknowledgments

This work was funded by the Climate Science for a Sustainable Energy Future (CSSEF) Program under the Biological and Environmental Research (BER) Office in the U.S. Department of Energy. The authors specifically acknowledge the Program Manager, Dr. Dorothy Koch, and the leadership of CSSEF, including Dr. Stephen Klein, Dr. William Collins, and Dr. David Bader. Finally, we thank the LLNL computational group involved in generating the runs of the CAM 5 model, including John Tannahill and Jim Boyle.

Contents

1	Introduction	11
1.1	Community Atmosphere Model 5	12
1.2	Table of parameters [LLNL & PNNL].....	12
1.3	Metrics	13
1.4	Ensemble design	14
	LLNL ensemble	14
	PNNL ensemble	14
1.5	Sampling methods	14
1.5.1	Latin Hypercube Sampling [SNL]	14
1.5.2	Quasi Monte Carlo [PNNL]	15
2	Methods	17
2.1	Surrogate methods	17
2.1.1	Generalized linear models [PNNL].....	17
2.1.2	MARS	17
2.1.3	Gaussian process models [LLNL & SNL]	18
2.2	Sensitivity methods	19
2.2.1	Correlation analysis [SNL & PNNL]	19
2.2.2	Variance based decomposition and Sobol' Sensitivity Indices [LLNL & SNL]	20
3	Results	23
3.1	SNL Results	24

3.2	PNNL Results	28
3.3	LLNL Results	34
4	Conclusions	47
4.1	Joint sensitivity analyses	47
	References	49

List of Figures

1.1	Table of input parameters varied for the studies performed in this report	12
1.2	Seven regions of interest investigated in this study. There are the six regions shown, and the last region, REG06, is the +/- 40-degree band around the equator (40S to 40N).	13
3.1	Correlation with respect to all harmonics, all regions, all seasons, LLNL data	24
3.2	VBD sensitivity indices with respect to all harmonics, all regions, all seasons, LLNL data	25
3.3	Correlation with respect to all harmonics, all regions, all seasons, PNNL data	25
3.4	VBD sensitivity indices with respect to all harmonics, all regions, all seasons, PNNL data	26
3.5	Global sensitivity indices with respect to all harmonics, all regions, all seasons, for both LLNL and PNNL data	26
3.6	Global sensitivity indices with respect to precipitation percentiles, all regions, all seasons, for both LLNL and PNNL data	27
3.7	R-squared values for Generalized Linear Model fits with respect to diurnal cycle harmonics magnitude and phase and 95th percentile, for both PNNL and LNNL data	29
3.8	Contribution of each input parameter's uncertainty to total output variance, for the Mountain region REG01, all seasons	30
3.9	Contribution of each input parameter's uncertainty to total output variance, for the Tropics region REG06, all seasons	31
3.10	Contribution of each input parameter's uncertainty to total output variance, for all parameters and all regions, for PNNL precipitation metrics.	32
3.11	Contribution of each input parameter's uncertainty to total output variance, for all parameters and all regions, for LNNL precipitation metrics.	32
3.12	Correlation of each input parameter to outputs for all parameters and all regions, for PNNL precipitation metrics.	33

3.13	Correlation of each input parameter to outputs for all parameters and all regions, for LLNL precipitation metrics.....	33
3.14	Regional average variance-explained of the 4 harmonics of the diurnal cycle by labs and seasons.	34
3.15	GPM fits for the first two harmonics in MMA, JJA in the SGP region	35
3.16	MARS fits for the first two harmonics in MMA, JJA in the SGP region	36
3.17	R-squared values for precipitation metrics in MMA, JJA in the SGP region, based on LLNL data, PNNL data, and the joint data	37
3.18	Contour plot of GPM predictions. The response contours show the GPM emulation of the first harmonic magnitude in the SGP region 7 in the JJA season.	38
3.19	Sobol' sensitivity indices for the magnitude of the 1st harmonic in region SGP in season JJA using GPMs trained on the PNNL data (top), the LLNL data (middle), and using both the LLNL and PNNL data (bottom).	40
3.20	Sobol' sensitivity indices for the magnitude of the 1st harmonic in region SGP in season JJA using MARS surrogates trained on the PNNL data (top), the LLNL data (middle), and using both the LLNL and PNNL data (bottom).	41
3.21	Sobol' sensitivity indices for metrics in region SGP in season JJA using GPMs. ...	42
3.22	Sobol' sensitivity indices for four metrics in two regions and in two seasons using GPMs. The results have been filtered so that metrics where the Sobol' indices are less than 0.01 are colored grey and results are eliminated for GPMs with R-squared values less than 0.5	43
3.23	Sobol' total sensitivity indices averaged across metrics in each region/season for PNNL, LLNL, and joint LLNL/PNNL study. The metrics where averaged together using weights based on the GPM's R^2	44
3.24	Averaged Sobol' indices across all regions and metrics, based on PNNL data, LLNL data, and joint data	45
4.1	Ranking of CAM5 model parameters by different laboratories. Summary of downselect list: parameters highlighted in green should definitely be included in further 1° studies, those in red should be eliminated, and those in yellow perhaps included.	48

Chapter 1

Introduction

The overall objectives of the Climate Science for a Sustainable Energy Future (CSSEF) program are to develop:

- The capability to thoroughly test and understand the uncertainties in the overall model and its components as they are being developed;
- Major scientific advances in the components that will achieve greater fidelity in modeling feedbacks in the climate system;
- Development of model evaluation procedures that allow the rapid ingest of observational data for model and component evaluation;
- Flexible dynamical cores that enable fine-scale simulations; and
- Early adaptation of the model algorithms and code to the next generation of computers.

The focus on uncertainty quantification involves sensitivity analysis: the capability to determine which input parameters have a major influence on the output responses of interest. This report presents some initial sensitivity analysis results. In the 2011-2012 timeframe, three laboratories (Lawrence Livermore National Laboratory (LNNL), Sandia National Laboratories (SNL), and Pacific Northwest National Laboratory (PNNL)) worked in collaboration to perform sensitivity analyses of a set of CAM5, 2° runs, where the response metrics of interest were precipitation metrics. The three labs performed their sensitivity analysis (SA) studies separately and then compared results. Overall, the results were quite consistent with each other although the methods used were different. Thus, we feel that this exercise provided a robust analysis approach.

In general, performing sensitivity analysis for expensive computational simulations with many parameter values is not a trivial task. A paper in the *Journal of Geophysical Research* by A. Saltelli [7] indicates that many sensitivity analyses use derivative-based approaches or methods that vary one parameter at a time (One at a Time or OAT). Saltelli discusses limitations of such approaches: they only explore a reduced portion of the input space and they typically do not account for parameter interactions. For models such as climate models that are highly nonlinear and have effects that are non-additive in the parameters, Saltelli recommends global sensitivity analysis approaches to account for the full effects of parameters on outputs. Note that global methods generally vary

multiple parameters simultaneously. Also note that sensitivity analysis is often the first step to further analyses such as uncertainty quantification and calibration (parameter estimation or parameter tuning). For an overview of global sensitivity analysis methods, we recommend [8] and [9].

1.1 Community Atmosphere Model 5

1.2 Table of parameters [LLNL & PNNL]

Thirty-two parameters were varied for this analysis, listed in Figure 1.1. The parameters relating to cloud microphysics were varied in the set that PNNL ran, and other atmospheric parameters were varied in the set that LLNL ran. There were some parameters varied in both, as denoted with “B” in the last column in Figure 1.1.

#	Parameter Name	Range			Description	Sampled By	Scale
		Low	Default	High			
1	dust_emis_fact	0.21	0.35	0.86	Dust emission tuning factor	B	lin
2	rhminh	0.65	0.80	0.85	Threshold RH for fraction high stable clouds	L	lin
3	rhminl	0.80	0.8875	0.99	Threshold RH for fraction low stable clouds	L	lin
4	ai	350.0	700.0	1400.0	Fall speed parameter for cloud ice	B	lin
5	as	5.86	11.72	23.44	Fall speed parameter for snow	B	lin
6	cdnl	eps+0.0	eps+0.0	eps+10.0e+6	Cloud droplet number limiter	B	log
7	dcs	100.0e-6	400.0e-6	500.0e-6	Autoconversion size threshold for ice to snow	B	lin
8	eii	0.001	0.1	1.0	Collection efficiency aggregation of ice	L	log
9	qcvr	0.5	2.0	5.0	Inverse relative variance of sub-grid cloud water	L	log
10	a2l	10.0	30.0	50.0	Moist entrainment enhancement parameter	L	lin
11	wsubimax	0.1	0.2	1.0	Maximum sub-grid vertical velocity for ice nucleation	L	lin
12	wsubmin	0.0	0.2	1.0	Minimum sub-grid vertical velocity for liquid nucleation	B	lin
13	criqc	0.5e-3	0.7e-3	1.5e-3	Maximum updraft condensate	L	lin
14	kevp	1.0e-6	2.0e-6	20.0e-6	Evaporative efficiency	L	log
15	rkm	8.0	14.0	16.0	Fractional updraft mixing efficiency	L	lin
16	rpen	1.0	5.0	10.0	Penetrative updraft entrainment efficiency	L	log
17	alfa	0.05	0.10	0.60	Initial cloud downdraft mass flux	L	log
18	c0_lnd	1.0e-3	0.0059	0.01	Deep convection precipitation efficiency over land	L	log
19	c0_ocr	1.0e-3	0.045	0.1	Deep convection precipitation efficiency over ocean	L	log
20	dmpdz	[0.2e-3]	[1.0e-3]	[2.0e-3]	Parcel fractional mass entrainment rate	L	log
21	ke	0.5e-6	1.0e-6	10.0e-6	Evaporation efficiency parameter	L	log
22	tau	1800.0	3600.0	28800.0	Convective time scale	L	log
23	refindex_aer_sw	0.001	0.005	0.01	Visible imag refractive index for dust	P	lin
24	sol_factic	0.2	0.4	0.8	Interstitial aerosol in convective wet removal tuning factor	P	lin
25	num_a1_surf_emis_fact	0.3	1.0	5.0	Number emission scaling factor for fossil fuel aerosol	P	lin
26	soag_emis_fact	0.5	1.5	2.0	SOA (g) emission scaling factor	P	lin
27	sst_emis_fact	0.5	1.0	2.0	Sea salt emission tuning factor	P	lin
28	sol_facti	0.5	1.0	1.0	Solubility factor for cloud-borne aerosols in stratiform clouds	P	lin
29	emis_so2_fact	0.0	1.0	2.0	emission tuning factor for SO2	P	lin
30	emis_bc_fact	0.0	1.0	3.0	emission tuning factor for BC	P	lin
31	emis_pom_fact	0.0	1.0	3.0	emission tuning factor for POM	P	lin
32	emis_so4f_fact	0.0	0.025	0.05	emission tuning factor for sulfate	P	lin

Figure 1.1. Table of input parameters varied for the studies performed in this report

Table 1.1. Response Metrics

7 Regions	4 Seasons plus Annual	Precipitation Metrics
REG01 = Mountains REG2 = High Plain REG03 = Mid Plain REG04 = Low Plain REG05 = South East REG06 = Equator Band 40S-40N REG07 = Southern Great Plains	Winter DJF Spring MAM Summer JJA Fall SON Annual ANN	Magnitude of first four harmonics of diurnal hydrological cycle Phase of first four harmonics of diurnal hydrological cycle Ave. daily precip. percentiles: 25%, 50%, 75%, 95%

1.3 Metrics

In these data sets, 1145 LLNL runs and 256 PNNL runs were performed. The metrics were computed using 5 years of hourly precipitation output. The study focused on two aspects of precipitation. The diurnal metrics of the hydrological cycle were calculated, including the magnitude and phase of the first harmonics of the diurnal cycle. These harmonics were calculated for each quarter (DJF, MAM, JJA, SON) as well as annually, for each of seven regions. The regions are shown in Figure 1.2. The precipitation quantiles were also calculated, including the 25%, 50%, 75%, and 95% precipitation quantiles. The different response metrics are shown in Table 1.1. There were 420 responses calculated for each CAM5 model run (7 regions * 5 time periods * 12 metrics (4 harmonic magnitudes, four harmonic phases, and four precipitation percentiles)). With this large volume of response metrics, we had to develop approaches to aggregate the individual sensitivities from a particular response.

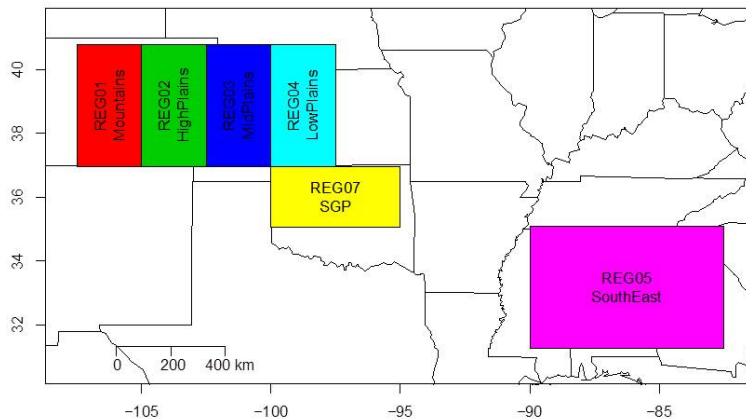


Figure 1.2. Seven regions of interest investigated in this study. There are the six regions shown, and the last region, REG06, is the +/- 40-degree band around the equator (40S to 40N).

1.4 Ensemble design

Separate ensemble runs were chosen to be performed at LLNL and at PNNL. The LLNL runs focused on parameters governing the atmosphere model, while the PNNL runs focused on parameters related to aerosols, but there was some overlap.

LLNL ensemble

The LLNL runs initially involved a Latin Hypercube sampling (LHS) study of 220 runs. This number was determined as ten times the number of parameters (22 for LLNL). Five separate LHS runs of 220 samples each were performed, for a total of 1100 runs. Then, one additional run involving parameters at their nominal values and two endpoints (one-at-a-time variations) was performed, for a total of 45 runs. The overall total was 1145 runs.

PNNL ensemble

The PNNL ensemble involved 256 runs, generated by a quasi Monte Carlo (QMC) sample. These 256 runs involved samples over 16 parameters.

1.5 Sampling methods

1.5.1 Latin Hypercube Sampling [SNL]

The most common method of incorporating uncertainty into simulations is to characterize uncertain input parameters with specific probability distributions, sample from those distributions, run the model with the sampled values, and do this repeatedly to build up a distribution of the outputs. Since computational simulations are often expensive, it is not always feasible to use random sampling to generate sufficiently large sample sizes. Thus, other methods have been developed. A good alternative to random sampling is Latin Hypercube Sampling (LHS) [McKay et al., Iman and Conover 1980]. LHS is a stratified sampling method where the support of the distribution is divided into strata or bins. Each stratum is chosen to be equally probable, so that the strata are of equal length for uniform distributions but of unequal length for normal distributions, for example: the strata near the center of normal distributions are shorter than the strata near the tails. In Latin Hypercube Sampling, each uncertain variable is divided into N segments of equal probability, where N is the number of samples requested. For each of the uncertain variables, a sample is selected randomly from each of these equal probability segments. These N values for each of the individual parameters are then combined in a shuffling operation to create a set of N parameter vectors with a specified correlation structure. A feature of the resulting sample set is that *every row and column in the hypercube of partitions has exactly one sample*. Since the total number of

samples is exactly equal to the number of partitions used for each uncertain variable, an arbitrary number of desired samples is easily accommodated (as compared to less flexible approaches in which the total number of samples is a product or exponential function of the number of intervals for each variable, i.e., many classical design of experiments methods).

The stratification approach in LHS serves to force a better sampling across the entire distribution and eliminate some of the clustering of sample points often seen in random sampling. For multidimensional sampling, it also serves to achieve a good "mixing" of sample values from different inputs. For example, you would not want the sample in strata 1 from input A to be paired with the sample in strata 1 from input B. Instead, you want the pairing of the strata to be performed in such a way to generate multi-dimensional samples that are "well-mixed" or randomized. Pairing algorithms have been designed to achieve this [Iman and Conover, 1982] and generate sample with a user-specified correlation structure. Finally, LHS is more efficient than pure Monte Carlo in the sense that it requires fewer samples to achieve the same accuracy in statistics (variance of the mean, for example). [Owen, Stein] If the function being sampled is additive, meaning it can be decomposed into additive functions of the individual input parameters, then the advantages of LHS are the greatest. For further information on the method and its relationship to other sampling techniques, one is referred to the works by McKay, et al. [6], Iman and Shortencarier [4], and Helton and Davis [3].

1.5.2 Quasi Monte Carlo [PNNL]

Regular Monte Carlo (MC) sampling is often insufficient because it generates redundant sampling points (clumps) and cannot fill the parameter space effectively. This may result in wasting computational time and unreliable sensitivity analysis. Quasi-Monte Carlo (QMC) methods use quasi-random (also known as low-discrepancy) sequences instead of random or pseudo-random numbers. Unlike pseudo-random sequences, quasi-random sequences do not attempt to imitate the behavior of random sequences. Instead, the elements of a quasi-random sequence are designed such that they are better dispersed than random sequences. There are a number of QMC sequences including Halton and Hammersley sequences. Many of the quasi MC sequences are based on a prime number. For further information on Quasi-Monte Carlo sequences, see [5].

Chapter 2

Methods

In general, sensitivity analysis methods require large numbers of function evaluations, typically greater than the number of actual CAM5 model runs that were performed for this study. Thus, all of the approaches utilized surrogates (also called meta-models or emulators) of the CAM5 model. The purpose of constructing a surrogate is so that it can be evaluated easily and cheaply. The following section discusses the surrogates that were employed in these studies.

2.1 Surrogate methods

2.1.1 Generalized linear models [PNNL]

The generalized linear model (GLM) is a flexible generalization of ordinary linear regression that allows for response variables that have other than a normal distribution. The GLM generalizes linear regression by allowing the linear model to be related to the response variable via a link function and by allowing the magnitude of the variance of each measurement to be a function of its predicted value. (need more)

2.1.2 MARS

MARS, multivariate adaptive regression splines, are credited to [2]. The form of the MARS model is based on the following expression:

$$\hat{f}(\mathbf{x}) = \sum_{m=1}^M a_m B_m(\mathbf{x}) \quad (2.1)$$

where the a_m are the coefficients of the truncated power basis functions B_m , and M is the number of basis functions. The MARS software partitions the parameter space into subregions, and then applies forward and backward regression methods to create a local surface model in each subregion. The result is that each subregion contains its own basis functions and coefficients, and the subregions are joined together to produce a continuous surface model.

MARS is a nonparametric surface fitting method and can represent complex multimodal data trends. The regression component of MARS generates a surface model that is not guaranteed to pass through all of the response data values. Thus, like the quadratic polynomial model, it provides some smoothing of the data.

2.1.3 Gaussian process models [LLNL & SNL]

The set of interpolation techniques known as Kriging, also referred to as Gaussian Processes, were originally developed in the geostatistics and spatial statistics communities to produce maps of underground geologic deposits based on a set of widely and irregularly spaced borehole sites[1]. Gaussian Process models are now widely used in response surface modeling, to “emulate” complex computer codes [Sacks et al.] The recent book by Rasmussen and Williams provides a good overview of Gaussian process models. [Rasmussen and Williams]. Building a Gaussian process model typically involves the

1. Choice of a trend function,
2. Choice of a correlation function, and
3. Estimation of correlation parameters.

A Gaussian process emulator, $\hat{f}(\underline{x})$, consists of a trend function (frequently a least squares fit to the data, $\underline{g}(\underline{x})^T \underline{\beta}$) plus a Gaussian process error model, $\varepsilon(\underline{x})$, that is used to correct the trend function.

$$\hat{f}(\underline{x}) = \underline{g}(\underline{x})^T \underline{\beta} + \varepsilon(\underline{x})$$

This represents an estimated distribution for the unknown true surface, $f(\underline{x})$. The error model, $\varepsilon(\underline{x})$, makes an adjustment to the trend function so that the emulator will interpolate, and have zero uncertainty at, the data points it was built from. The covariance between the error at two arbitrary points, \underline{x} and \underline{x}' , is modeled as

$$\text{Cov}(y(\underline{x}), y(\underline{x}')) = \text{Cov}(\varepsilon(\underline{x}), \varepsilon(\underline{x}')) = \sigma^2 r(\underline{x}, \underline{x}').$$

Here σ^2 is known as the unadjusted variance and $r(\underline{x}, \underline{x}')$ is a correlation function. Gardar and Don: We should decide on a convention for notation before we write more: I will include the formulas for the prediction mean and variance, but want to first get a consensus on notation. There are three main steps to creating and using a Gaussian process model: (1) define the mean function, (2) define the covariance function and estimate the hyperparameters governing the covariance function, (3) perform the prediction calculations at new points. There are many numerical issues involved in determining the length-scale parameters governing the covariance function; the interested reader should consult (cites). There are two main approaches for determining the length-scale parameters in the covariance function. One is to use maximum likelihood estimation, where one maximizes the likelihood function. This results in point estimates of the covariance parameters. The other approach is to use Monte Carlo Markov Chain (MCMC) sampling to generate posterior distributions on the hyperparameters which govern the covariance function and the mean function. The

assumption of zero mean GPs is often made, so the Bayesian updating only involves hyperparameters governing the covariance function. Since these may be quite complicated, one usually still needs a MCMC sampling method to generate the posterior.

2.2 Sensitivity methods

Our ultimate goal is to understand the sensitivity of the various metrics considered with respect to the uncertain input parameters. The edited volume by Saltelli, Chan and Scott (2000) and the paper Saltelli, Tarantola and Campoingo (2000) provide a good overview with application to this topic.

Our focus is on global sensitivity indices, which reflect the sensitivity of a quantity of interest with respect to the uncertain inputs when they are varied over the whole prior uncertainty range (versus at a particular value in the input space). For added robustness to our analysis, we report results from multiple sensitivity analysis methods, with some methods operating directly on the raw ensemble of simulations while others relying on a surrogate model.

2.2.1 Correlation analysis [SNL & PNNL]

Correlation refers to a statistical relationship between two random variables or two sets of data. In analysis of computer experiments, where an ensemble of simulation runs have been performed according to some type of experimental design, we have a set of results. The convention is to have each sample or run of the simulation be written on a separate row. For example, if N simulation runs were performed, with D inputs and P outputs, the resulting ensemble matrix would be of dimension $N \times (D+P)$. In this situation, we can perform a correlation analysis on the entire matrix. However, often the correlations between inputs and inputs are not interesting, especially if the sample design has been constructed so that the inputs are independent and thus the correlations between inputs are near zero. Likewise, the correlations between outputs and outputs may not be interesting, except in the case where some of the outputs are very strongly correlated and thus perhaps one can reduce the analysis by only focusing on a subset of outputs. The main focus of correlation analysis of computer experiments is the correlation between inputs and outputs. There are several types of correlations that can be calculated: simple, rank, and partial. Simple correlation measures the strength and direction of a linear relationship between variables. Simple correlation refers to Pearson's correlation coefficient, which is defined for two variables x and y as: $\text{Corr}(x, y) = \frac{\sum_i (x_i - \bar{x})(y_i - \bar{y})}{\sqrt{\sum_i (x_i - \bar{x})^2 \sum_i (y_i - \bar{y})^2}}$. The Pearson correlation is +1 in the case of a perfect positive (increasing) linear relationship, -1 in the case of a perfect decreasing (negative) linear relationship, and some value between -1 and 1 in all other cases. A simple correlation near zero means there is less of a relationship between the variables: they are close to being uncorrelated. Note that if two variables are independent, they will have zero correlation but the converse is not true: two variables may have zero or near-zero correlation but show a strong type of relationship. Rank correlations refer to correlations performed on the ranks of the data. Ranks are obtained by replacing

the actual data by the ranked values, which are obtained by ordering the data in ascending order. For example, the smallest value in a set of input samples would be given a rank 1, the next smallest value a rank 2, etc. Rank correlations are useful when some of the inputs and outputs differ greatly in magnitude: then it is easier to compare if the smallest ranked input sample is correlated with the smallest ranked output, for example. A rank correlation coefficient is also called a Spearman correlation. Partial correlation coefficients are similar to simple correlations, but a partial correlation coefficient between two variables measures their correlation while adjusting for the effects of the other variables. For example, if one has a problem with two highly correlated inputs and one output, the correlation of the second input and the output may be very low after accounting for the effect of the first input.

2.2.2 Variance based decomposition and Sobol' Sensitivity Indices [LLNL & SNL]

One of the more common, and successful sensitivity analysis methods are those based on variance decomposition of the response of interest with respect to the uncertain input parameters. In this case, one seeks to decompose the variance of a given response $V(y)$, where $y = f(x_1, \dots, x_p)$, as contributions from various sources, both due to a given input parameter alone and various level of interaction between input parameters (i.e. main effect, two-way interaction, etc.). This type of analysis mirrors analyses of variance (ANOVA) in the statistical literature.

If we assume that the distribution of the uncertain input parameters are independent, that is, $p(x_1, \dots, x_p) = \prod_{i=1}^p p_i(x_i)$, and that the response function $f(x)$ is square-integrable, then

$$V_0 \equiv V(y) = \sum_{i=1}^p V_i + \sum_{i<j} V_{ij} + \sum_{i<j<k} V_{ijk} + \dots + V_{1\dots p},$$

where

$$V_i \equiv V(E(y|x_i)) \quad \text{and} \quad V_{ij} \equiv V(E(y|x_i, x_j)) - V_i - V_j$$

and similarly for higher terms. Here, $y_i(\tilde{x}_i) \equiv E(y|x_i = \tilde{x}_i)$ denotes the conditional expectation of y given the i -th input (and averaging over the remaining inputs). Hence, V_i is simple the variance of the 1D function $y_i(\tilde{x}_i)$ with respect to the i -th input distribution, $p_i(\tilde{x}_i)$. Similarly, we define $V_{-i} = V(E(y|x_1, \dots, x_{i-1}, x_{i+1}, \dots, x_p))$; that is, the conditional variance of y given all the input except the i -th one.

Of main interest are Sobol' main and total effect sensitivity indices, defined as

$$S_i \equiv \frac{V_i}{V_0} \quad \text{and} \quad S_i^T \equiv \frac{V_0 - V_{-i}}{V_0},$$

respectively. Hence, S_i gives the fraction of the total variance explained by the i -th main effect alone (i.e., the contribution of the i -th input without any interactions to other inputs), while the total effect provides the fraction of the total variance explained by all terms involving the i -th term.

To give an example, if there are three inputs ($p = 3$), then

$$S_1^T = \frac{V_1 + V_{12} + V_{13} + V_{123}}{V_0} = S_1 + S_{12} + S_{13} + S_{123}.$$

Hence, S_i^T is a measure of the total (global) importance of the i -th input, while the difference between S_i^T and S_i gives a measure of how much the i -th input interacts with the remaining inputs.

Numerous methods have been proposed to estimate Sobol'-type of sensitivity indices, all of them relying on a clever sampling of the uncertain input parameters (see Saltelli, Chan, and Scott, 2000, for an overview). For example, one of the original methods to estimate S_i and S_i^T (Sobol's method) requires $2n(p+1)$ number of model evaluations, which are constructed from two different $n \times p$ LH-sampled input configurations. For $p = 22$ parameters (the LLNL study), this would call for a relatively large value of n , say 1,000, yielding 46,000 runs. More economic ways exist that cut the total number of runs by approximately half. However, this is simple not feasible with CAM5, even at the course resolution and short time integration used in the CSSEF study. The approach taken here is to use the ensemble of CAM5 simulations to train a surrogate model and sample the surrogate model in place of the simulator. The uncertainty in the resulting sensitivity indices is then both due to the sampling-based approach used to estimate the indices (which can be kept as small as desired) and the uncertainty in the surrogate model itself, which need to be assessed.

Chapter 3

Results

This chapter presents the results of the sensitivity analyses performed at the various laboratories. The goal of these studies was to downselect from the thirty-two parameters analyzed in the 2° ensembles to a more limited set of parameters (ideally, around 10) to be varied in higher-resolution 1° ensemble runs. This chapter first presents the results of each lab separately, then presents the aggregation of their work in the final section.

3.1 SNL Results

The group at SNL took the following approach: they used two global sensitivity analysis methods: correlation analysis and variance-based decomposition (VBD). They created Gaussian process model surrogates for the various metrics based on the parameter sets and CAM5 runs described in Chapter 1. They analyzed the LLNL and PNNL data separately, and they analyzed the harmonics of the diurnal cycle (magnitude and phase of the first four modes) separately from the percentiles of precipitation. The results were aggregated across regions and across metrics, first by LLNL vs. PNNL data and also by correlation vs. VBD analysis. Then, the results were combined to create a union of LLNL and PNNL data. This union of the significant variables allowed us to identify a set we can consider eliminating in the 1-degree nudged runs.

Figures 3.1 and 3.2 show the results of correlation analysis and VBD analysis for the harmonics for the LLNL ensemble. These figures show the percentage of times a parameter was considered significant, as measured by a correlation coefficient whose absolute value was greater than 0.5, or a variance-based main effect indices whose value was greater than 0.1. The percentage is taken across all regions, all seasons, and phase and magnitude of the harmonics. For example, in Figure 3.1, one can see that parameter 22 is important about 45% of the time. This parameter (from Figure 1.1) is tau, the convective time scale, which is known to play an important role in the precipitation. An important point to note is how similar Figures 3.1 and 3.2 are to each other: the important parameters are consistent across these two methods.

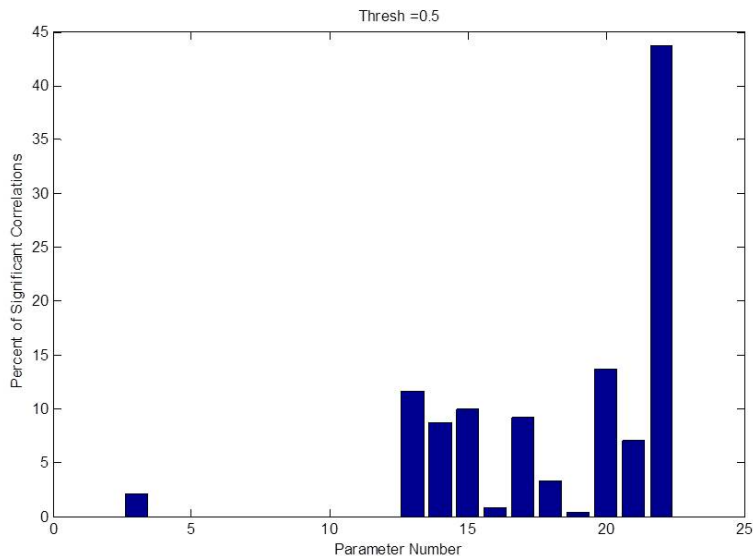


Figure 3.1. Correlation with respect to all harmonics, all regions, all seasons, LLNL data

Figures 3.3 and 3.4 show analogous results of correlation analysis and VBD analysis for the harmonics of the PNNL ensemble. Parameter number 4 for the PNNL ensemble is the most

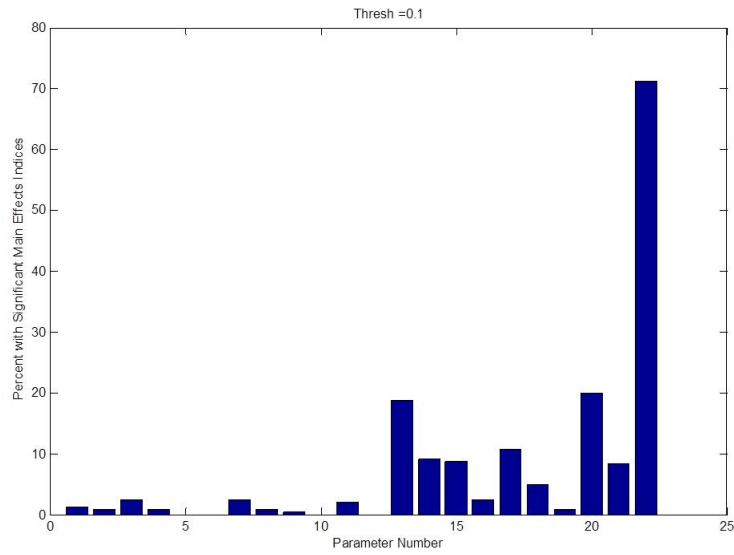


Figure 3.2. VBD sensitivity indices with respect to all harmonics, all regions, all seasons, LLNL data

significant, which is the cdnl, the cloud droplet number limiter (also called cldwatmi_cdn1). Again, we see that Figures 3.3 and 3.4 are very similar.

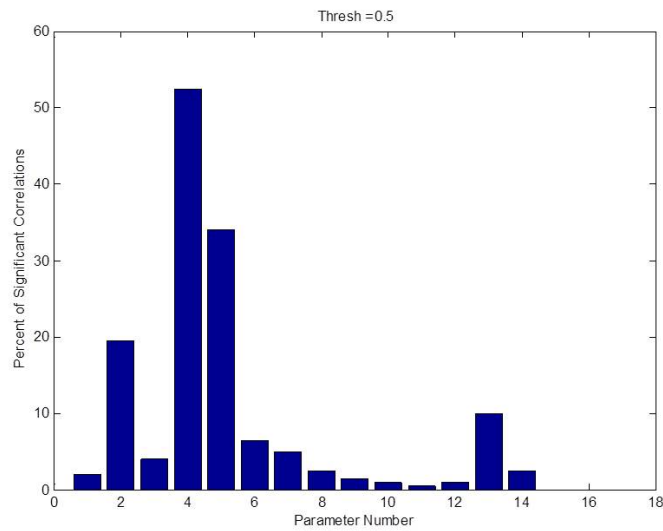


Figure 3.3. Correlation with respect to all harmonics, all regions, all seasons, PNNL data

The results of Figures 3.1 to 3.4 were aggregated: these aggregate results are shown in

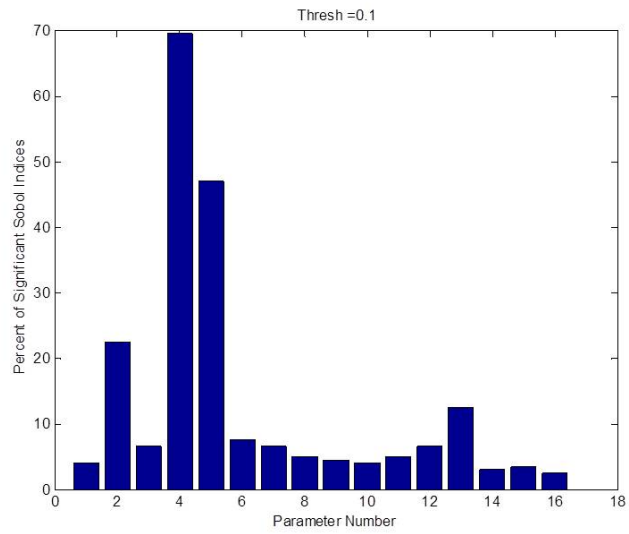


Figure 3.4. VBD sensitivity indices with respect to all harmonics, all regions, all seasons, PNNL data

Figure 3.5.

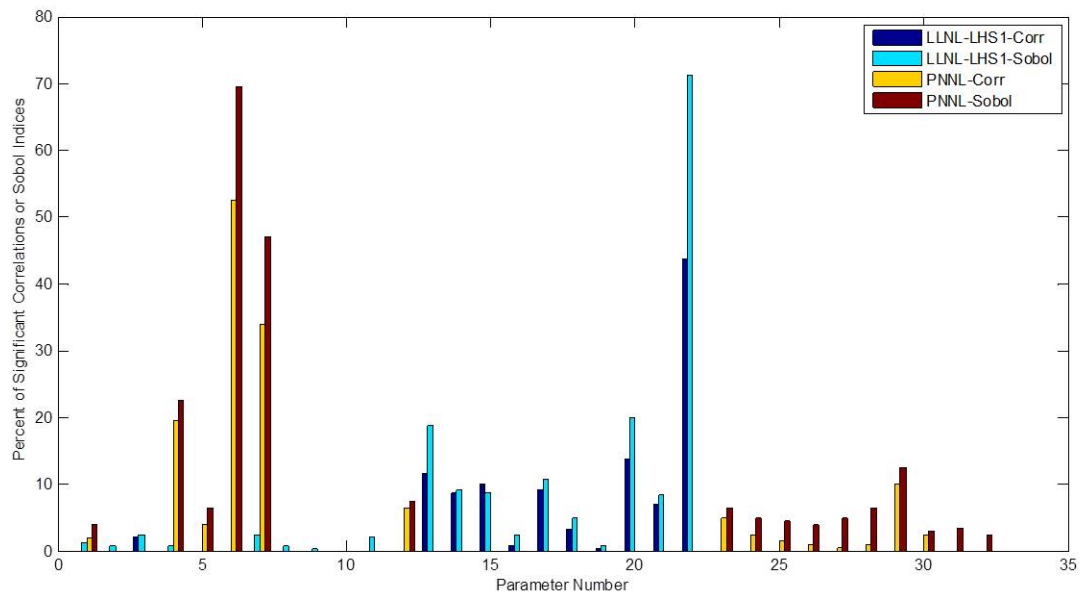


Figure 3.5. Global sensitivity indices with respect to all harmonics, all regions, all seasons, for both LLNL and PNNL data

Finally, a similar analysis was performed with respect to the precipitation percentiles. The results are similar to the results from the harmonics of the diurnal cycle, although more parameters were significant in the precipitation percentile data, especially for the LLNL data. In the interest of space, we only present the final aggregated result in Figure 3.6.

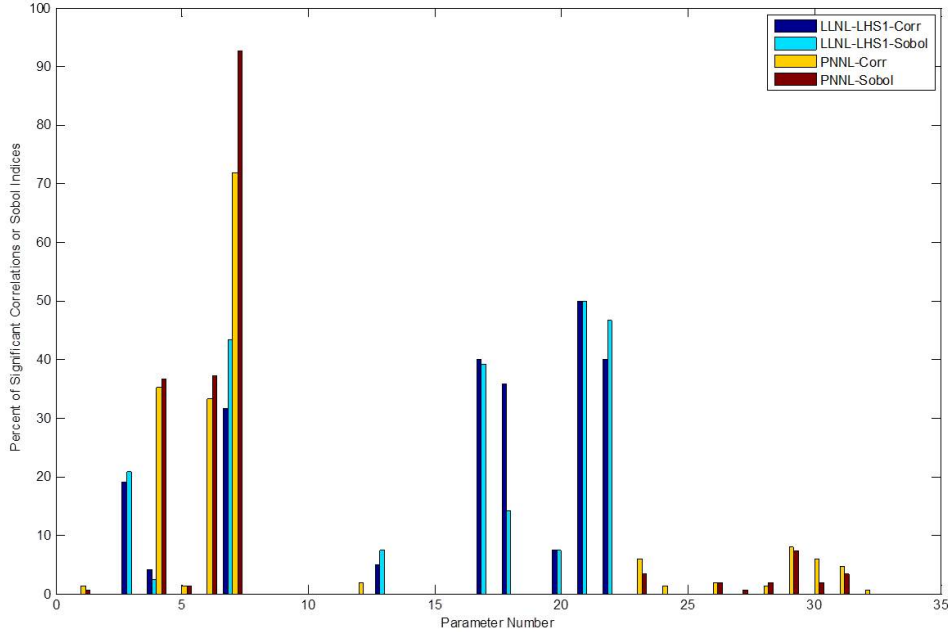


Figure 3.6. Global sensitivity indices with respect to precipitation percentiles, all regions, all seasons, for both LLNL and PNNL data

In summary, the SNL analyses demonstrated that correlation coefficients and Sobol' variance-based indices gave similar results within a particular data set. We did find that the important variables differed for harmonics and precipitation. For harmonics, the important variables were:

- LLNL: uwshcu_criq, zmconv_dmpdz, zmconv_tau
- PNNL: cldwatmi_ai, cldwatmi_cdn1, cldwatmi_dcs

For the precipitation percentiles, the important variables were:

- LLNL: cldwatmi_dcs, zmconv_alfa, zmconv_c0_lnd, zmconv_ke, zmconv_tau
- PNNL: cldwatmi_ai, cldwatmi_cdn1, cldwatmi_dcs

3.2 PNNL Results

PNNL developed generalized linear models (GLM) for the harmonics and the precipitation percentiles. The GLMs were used to calculate the percentage of response variance explained for various metrics, across various regions and in different seasons. The PNNL team plotted the results of the relative contributions of variance explained, and they also performed correlation analysis.

Figure 3.7 shows the results of various fits using the GLM. The metric shown in this figure is R-squared, the fraction of variance for an output variable explained or captured by GLM. R-squared takes values between zero and one, where a value of one typically means a “perfect fit” (e.g. the output is perfectly explained by the inputs). Note that R-squared is much smaller in DJF than in other seasons for both PNNL and LLNL data. The R-squared values for LLNL data are generally larger than for PNNL data, since the LLNL simulations cover more parameters related to macro- and micro-physics and shallow and deep convections, which all are important for precipitation diurnal cycle and extremes. The R-squared values for PNNL data are larger in the tropics (REG06) than other regions and higher for the harmonic magnitudes (MAG) than other variables.

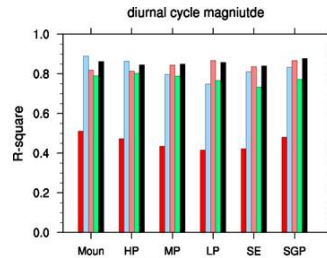
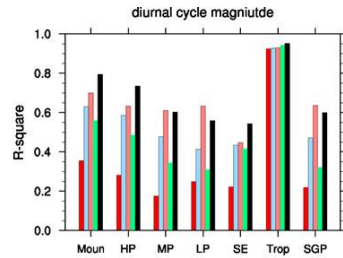
Figure 3.8 is a more detailed figure which shows the contribution of the individual parameters with respect to percent output variance explained for the magnitude of the harmonics. This is calculated for each of the 16 parameters, for 5 seasons (5 colors). The numbers on the x-axis are the relative contribution of each parameter’s uncertainty to the total variance of the harmonic magnitude in REG01. This type of plot can provide a lot of information for the sensitivity and variability/tendency of each parameter.

Figure 3.9 shows a similar plot, for results over the tropics.

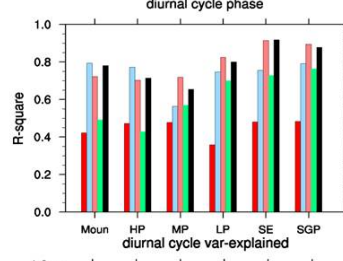
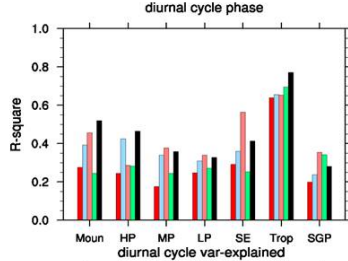
Figures 3.10 and 3.11 show aggregated results, where the color of each square denotes the percentage of variance explained for that parameter and metric combination. Note that the red squares denote the most important parameters. For example, the upper left hand plot in Figure 3.10 indicates that the dcs parameter is very important to explaining the variance of the 95th percentile of precipitation across almost all the regions, as shown by the red line in that Figure. These plots are very useful for aggregating information across metrics and across regions.

Finally, the PNNL team performed a correlation analysis, similar to what the SNL team did. Their results are shown for the PNNL and LLNL datasets in Figures 3.12 and 3.13.

GLM R-Square



PNNL data



LLNL data

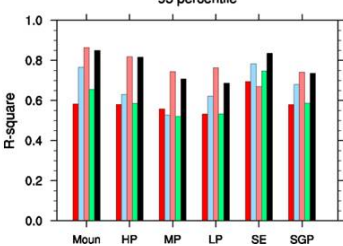
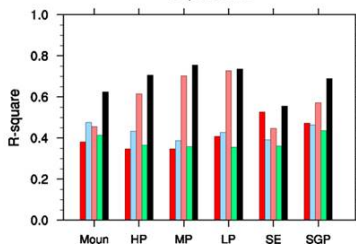
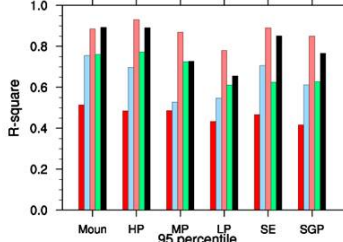
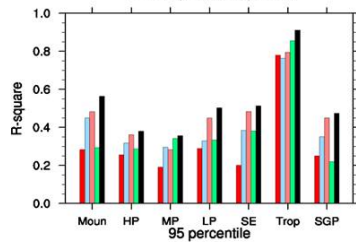


Figure 3.7. R-squared values for Generalized Linear Model fits with respect to diurnal cycle harmonics magnitude and phase and 95th percentile, for both PNNL and LLNL data

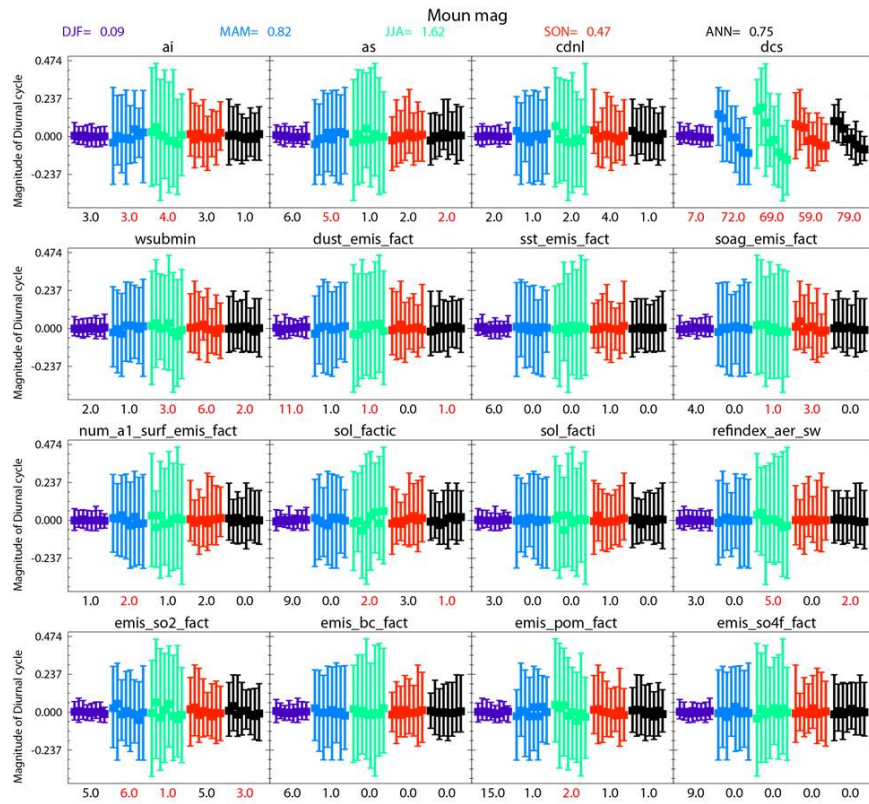


Figure 3.8. Contribution of each input parameter's uncertainty to total output variance, for the Mountain region REG01, all seasons

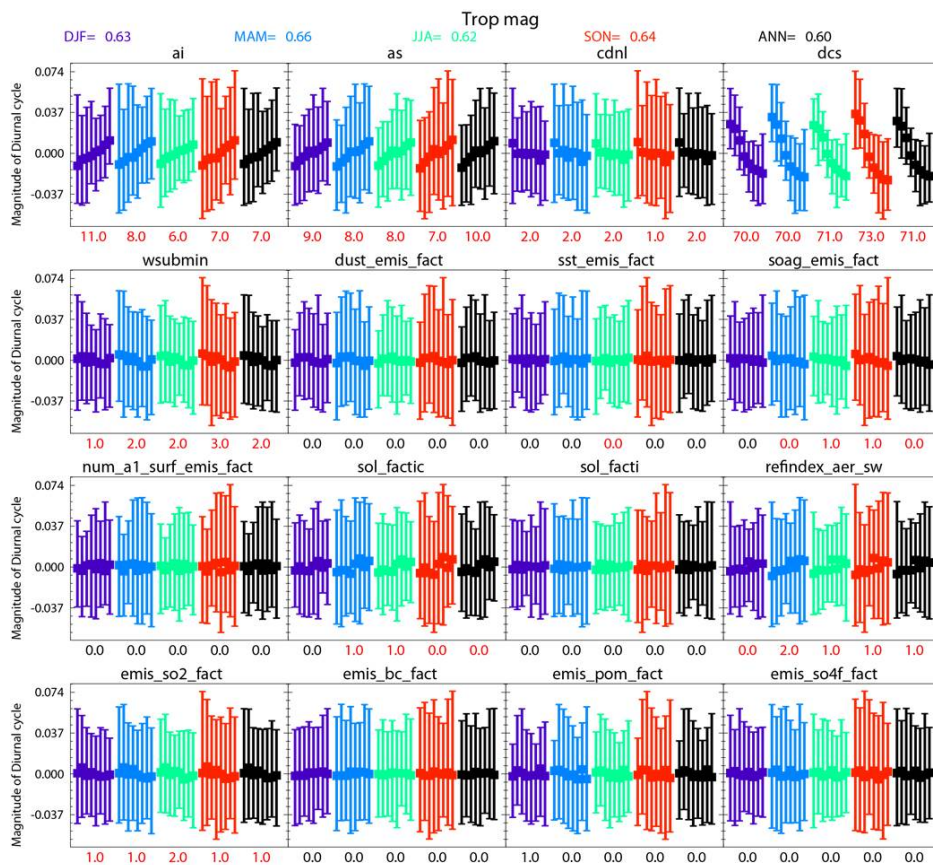


Figure 3.9. Contribution of each input parameter's uncertainty to total output variance, for the Tropics region REG06, all seasons

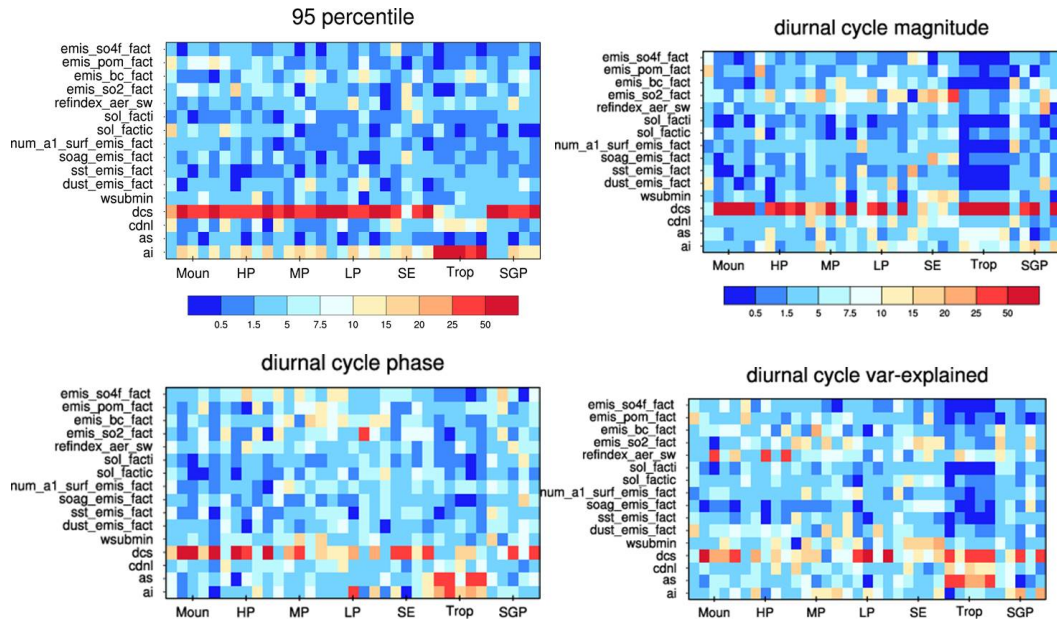


Figure 3.10. Contribution of each input parameter’s uncertainty to total output variance, for all parameters and all regions, for PNNL precipitation metrics.

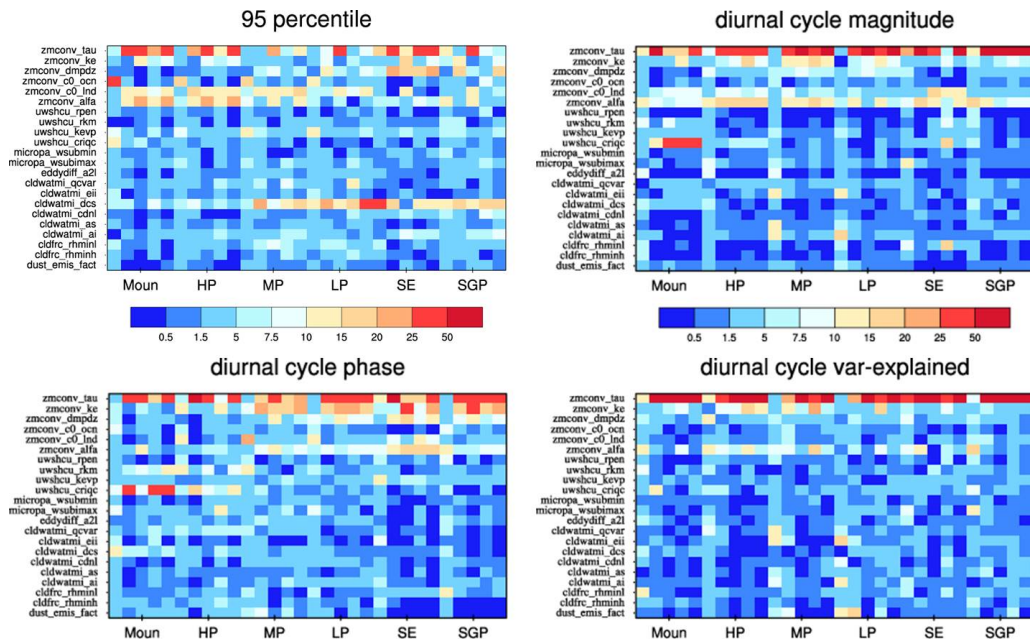


Figure 3.11. Contribution of each input parameter’s uncertainty to total output variance, for all parameters and all regions, for LNNL precipitation metrics.

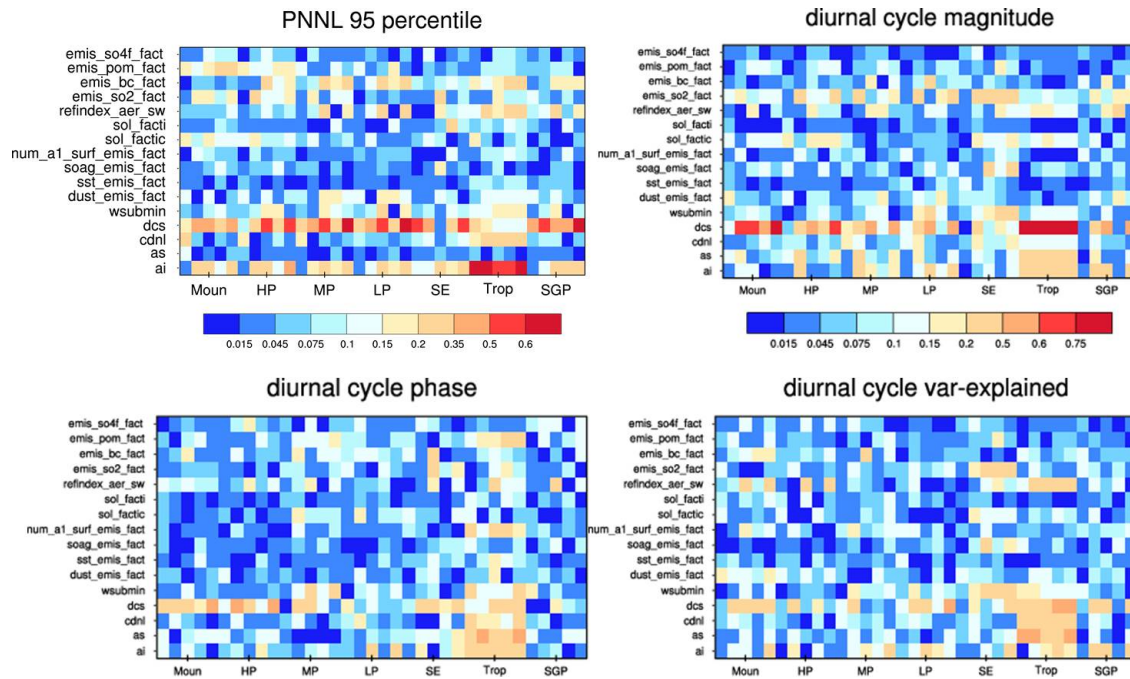


Figure 3.12. Correlation of each input parameter to outputs for all parameters and all regions, for PNNL precipitation metrics.

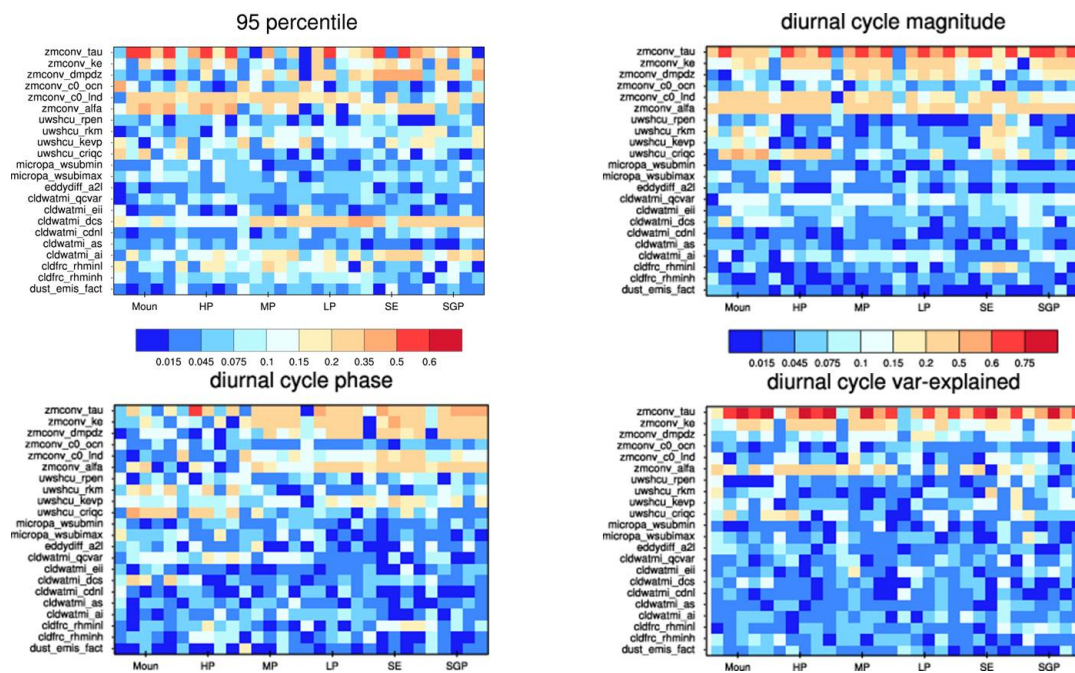


Figure 3.13. Correlation of each input parameter to outputs for all parameters and all regions, for LLNL precipitation metrics.

3.3 LLNL Results

The LLNL group created statistical emulators that were trained on PNNL, LLNL, and LLNL/PNNL data jointly. They used two types of surrogate models, Gaussian process models (GPM) and Multivariate Adaptive Regression Splines (MARS). The LLNL group used the emulators to analyze the response and perform the sensitivity analysis via Sobol’ indices. These indices were then aggregated across metrics, regions, and seasons to produce a ranked list of parameters.

Figure 3.14 shows the percent of variance explained by the first four harmonics. Note that most of the variance is explained by the first two harmonics and as such, all the following analysis focuses on the two first harmonics.

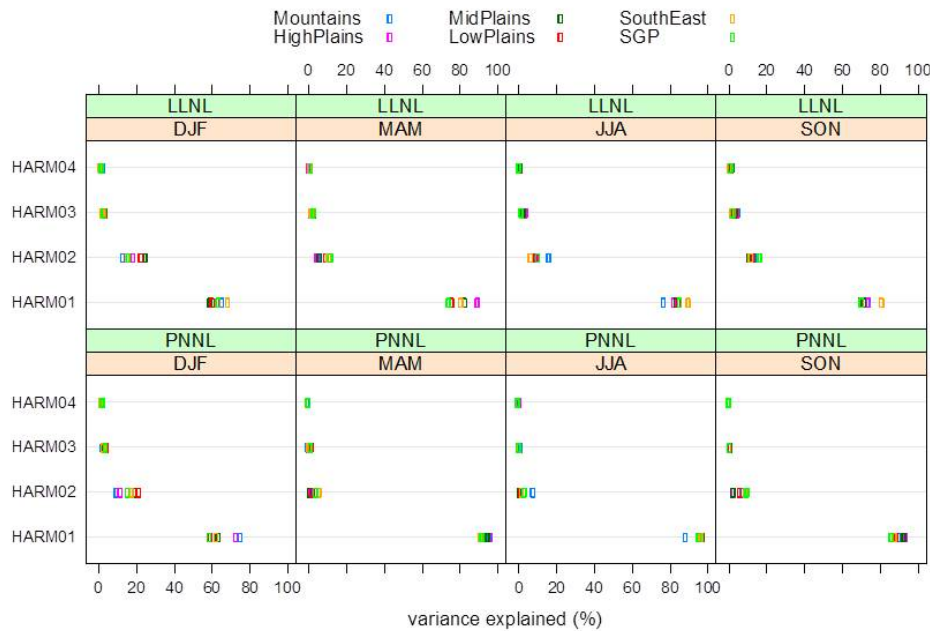


Figure 3.14. Regional average variance-explained of the 4 harmonics of the diurnal cycle by labs and seasons.

Further analysis of the harmonics and precipitation quantiles showed that the largest variation in the diurnal cycle was in the spring and summer seasons. The largest median precipitation (Q50) was in JJA and the largest Q95 was in MAM.

We now present detailed preliminary examination focusing on the MAM and JJA seasons for two different types of regions, the SGP (REG07) and the SouthEast (REG05) regions. The approach developed using these two regions and seasons is then applied to all six regions at the end.

The two emulators (GPMs and MARS) were trained separately first and then jointly on the LLNL and PNNL data. For the LLNL data, two sets of LHS samples were used ($2 \times 220 = 440$

runs) and the one set of one-at-a-time (45 runs) for a total of 465 runs. For the PNNL data, the single set of pseudo-random samples (256 runs) and one control run varying 16 inputs was used for a total of 257 runs.

Figure 3.15 shows the GPM predictions based on 440 runs (the training data). The plots in this figure show the predicted magnitudes (with 90 error bars) of the first two harmonics in MAM and JJA for the SGP region (REG07) for the 660 LLNL runs withheld from the training data. The cross-validated (CV) R-squared values are also shown, using 20-fold cross validation. The GPMs are more accurate at predicting the 1st harmonic. Figure 3.16 shows similar results for the MARS predictions also based on the 440 training data runs.

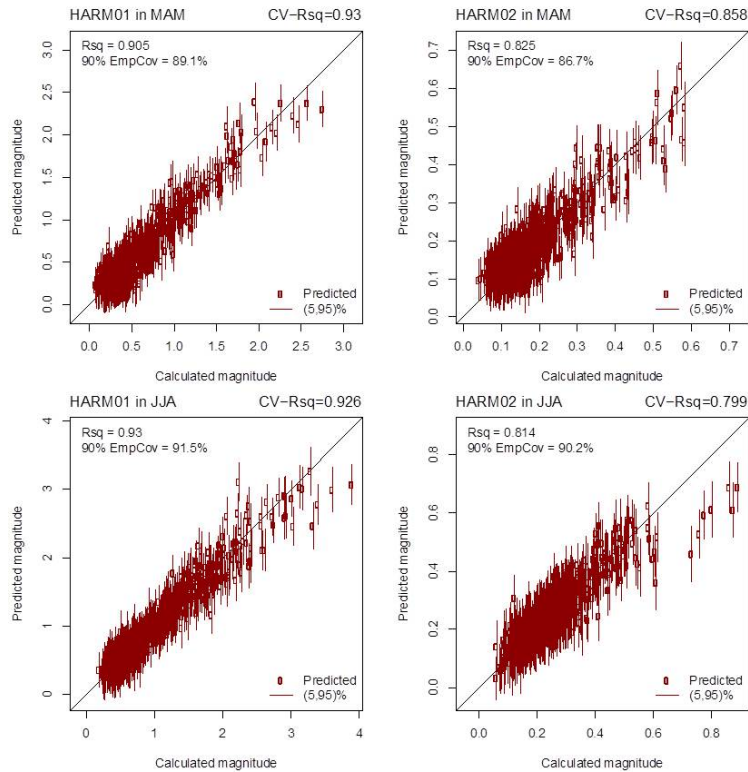


Figure 3.15. GPM fits for the first two harmonics in MMA, JJA in the SGP region

The R-squared metrics for the GPM and MARS models are shown in Figure 3.17. The GPMs are in general more accurate than MARS. In general, it is easier for the emulators to predict the Q50 (50%) of the precipitation output than the Q95 percentile. Also, it is easier to predict the magnitude than the phase of the harmonics of the diurnal cycle. Figure 3.17 shows the (20-fold) cross-validation R-squared values for GPM and MARS trained on each lab separately and jointly to all data. Note that both GPM and MARS have problem with the PNNL data, except for the Q50 metric.

A bi-variate contour plot of the GPM response for the magnitude of the first harmonic in the

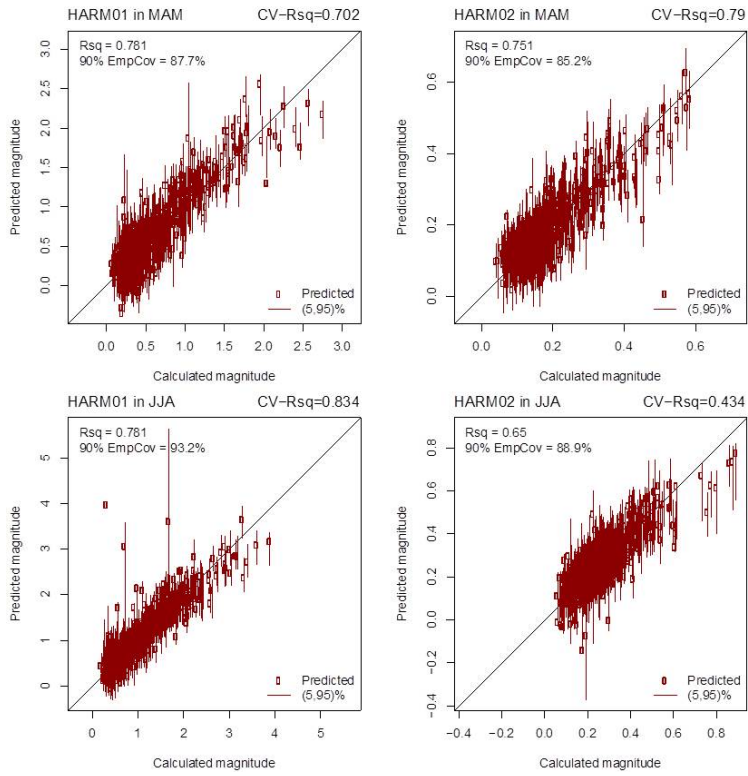


Figure 3.16. MARS fits for the first two harmonics in MMA, JJA in the SGP region

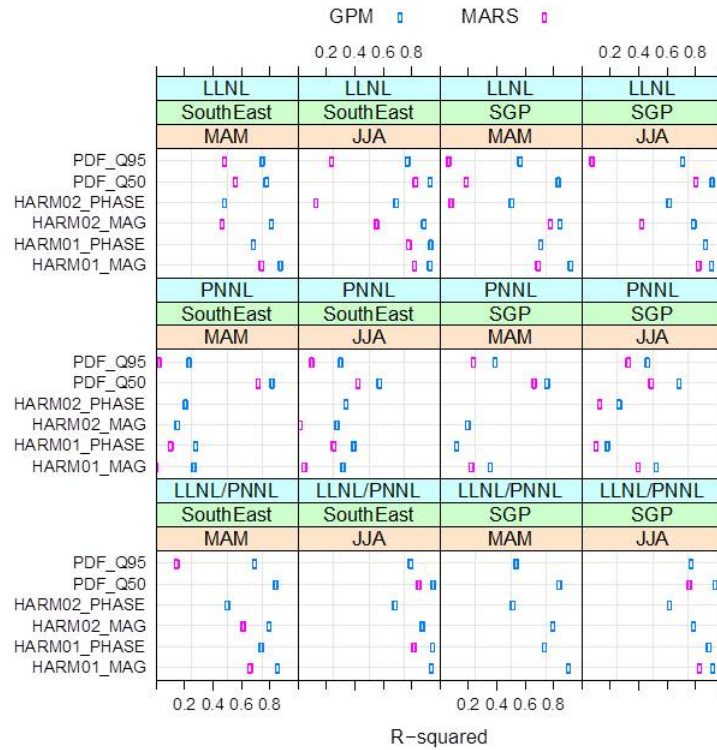


Figure 3.17. R-squared values for precipitation metrics in MMA, JJA in the SGP region, based on LLNL data, PNNL data, and the joint data

SGP region in the JJA season is shown in Figure 3.18. In this plot, the harmonic response is shown as a function of the six most sensitive inputs. In these plots, either one input (diagonal plots) or two (off-diagonal plots) are varied with the remaining inputs fixed at their default values (black circles). The true response is shown on the diagonal plots, where the LLNL response is denoted with a circle and the PNNL response by a triangle. The grey area shows 2-sigma prediction error bars. Overall, `zmconv_tau` is the most important parameter, although in the PNNL only data, `cdlwatmi_dcs` is the most important paramter.

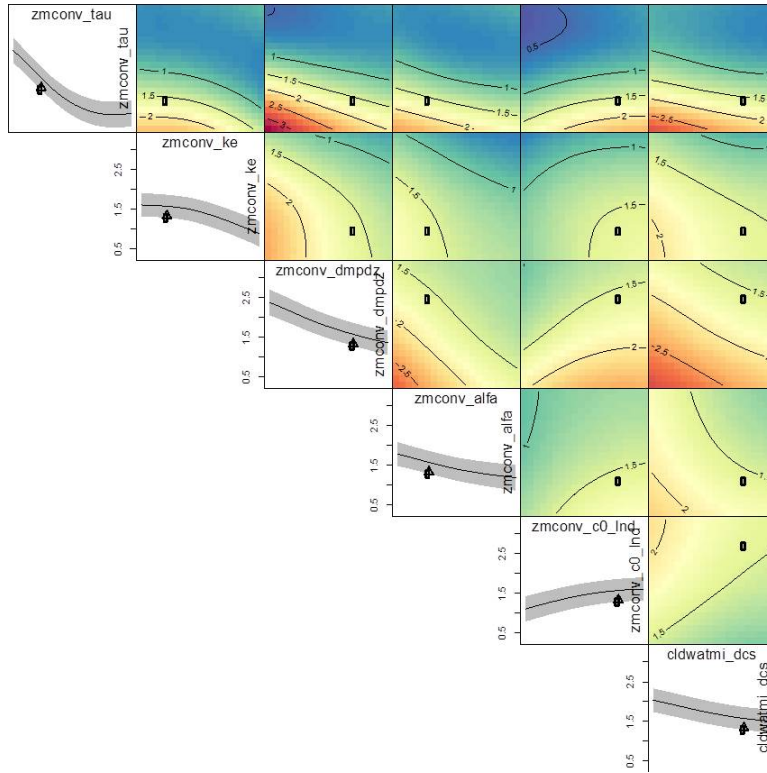


Figure 3.18. Contour plot of GPM predictions. The response contours show the GPM emulation of the first harmonic magnitude in the SGP region 7 in the JJA season.

The Sobol' main- and total-effect sensitivity indices were calculated using sampling-based (Monte Carlo) based approach based on the original method of Sobol' using two LH-sampled set of size $n = 10,000$ each (the total number of surrogate evaluations is then $n(2p + 2)$ where p is either 16 or 22 for PNNL and LLNL respectively). The estimated sensitivity indices were tested for Monte Carlo error using bootstrap techniques and were found to be relatively small. The sensitivity indices were also tested for error in the surrogate models by generating realizations from the GPM and by bootstrapping the MARS. As expected, for surrogate models with relatively low R^2 , the resulting indices had large standard deviation, which should be factored in the final results.

Recall that the main effect indices indicate the relative variance explained by the main-effect of each input variable, while the total effect indices indicate the relative variance explained by the main-effect and any interaction with other inputs for a given input. Figure 3.19 shows the Sobol' sensitivity indices for the magnitude of the 1st harmonic in region SGP in season JJA using GPMs trained on the PNNL data (top), the LLNL data (middle), and using both the LLNL and PNNL data (bottom). Figure 3.20 shows the same sensitivity indices, but based on a MARS surrogate instead of a GPM. We note some difference in the two set of estimates, as expected, but the most important input parameters are in each case are very similar (e.g., the top 4 parameters are identical and in the same order for the joint PNNL/LLNL case).

Figure 3.21 shows the total sensitivity indices for 6 different metrics in JJA for region SGP, showing that many of the parameters are not influential with respect to some of the metrics. Because the GPM and MARS surrogates are not very good emulators with respect to some of the metrics, the LLNL group showed the data in a slightly different way. Figure 3.22 shows sensitivity indices for four metrics in two regions and two seasons (based on GPMs), but the areas where the Sobol' indices are less than 0.01 are colored grey, and the plot only shows results for those metrics whose GPM has an R-squared value of greater than 0.5. The results are eliminated for the poorer emulators (e.g. those whose R-squared is less than 0.5). The GPMs were used rather than the MARS surrogates as they yielded higher R^2 on averaged.

To construct a single total sensitivity index for a given region/season, the sensitivity indices from multiple metrics were averaged using the GPMs' R^2 as weights, thus down-weighting sensitivity indices based on poorly fitted GPMs. The resulting region/season based sensitivity indices are shown in Figure 3.23 for 6 regions and 2 seasons. Finally, the indices were averaged across regions and seasons to form a single sensitivity index, which are summarized in Figure 3.24.

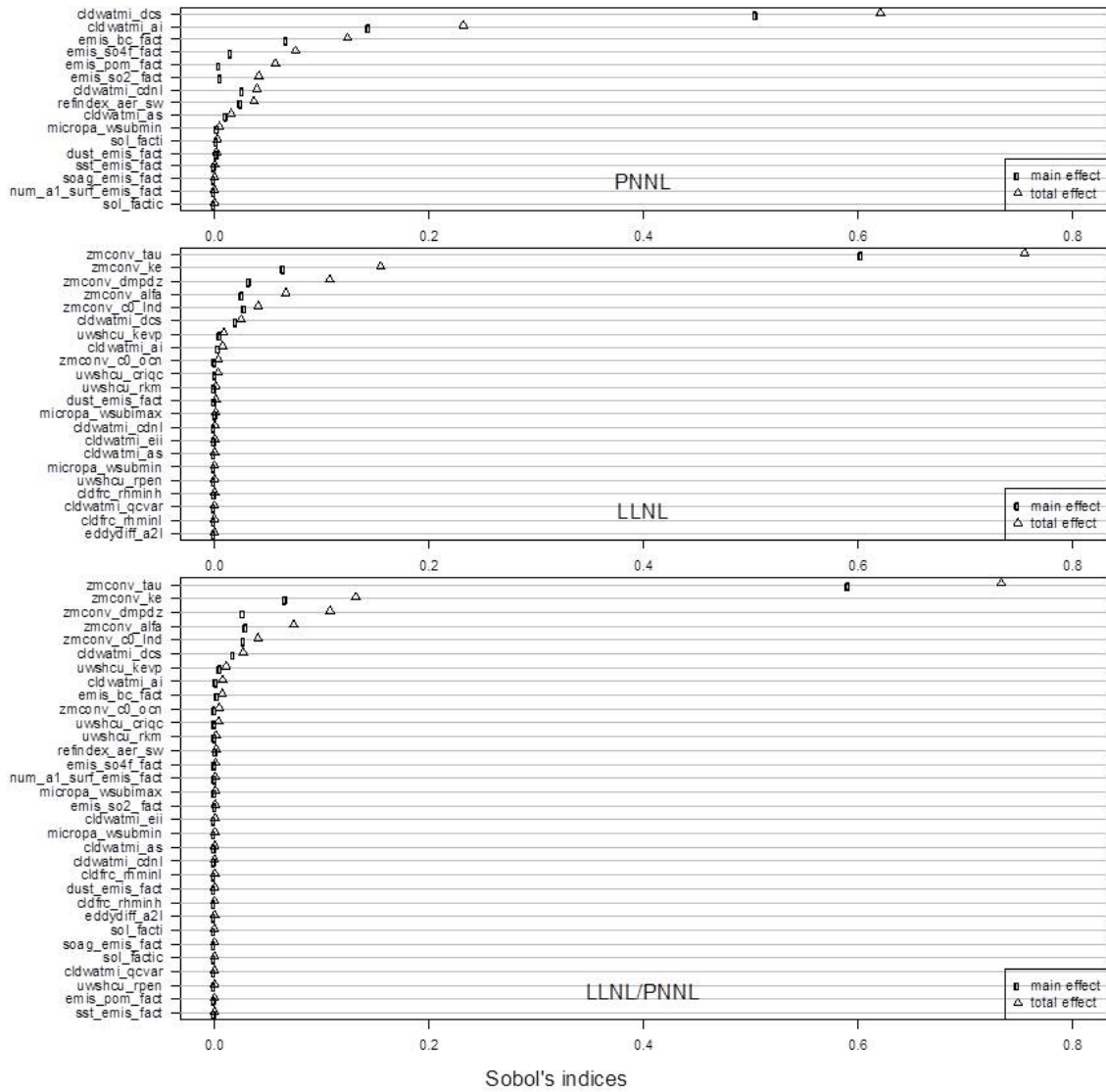


Figure 3.19. Sobol' sensitivity indices for the magnitude of the 1st harmonic in region SGP in season JJA using GPMs trained on the PNNL data (top), the LLNL data (middle), and using both the LLNL and PNNL data (bottom).

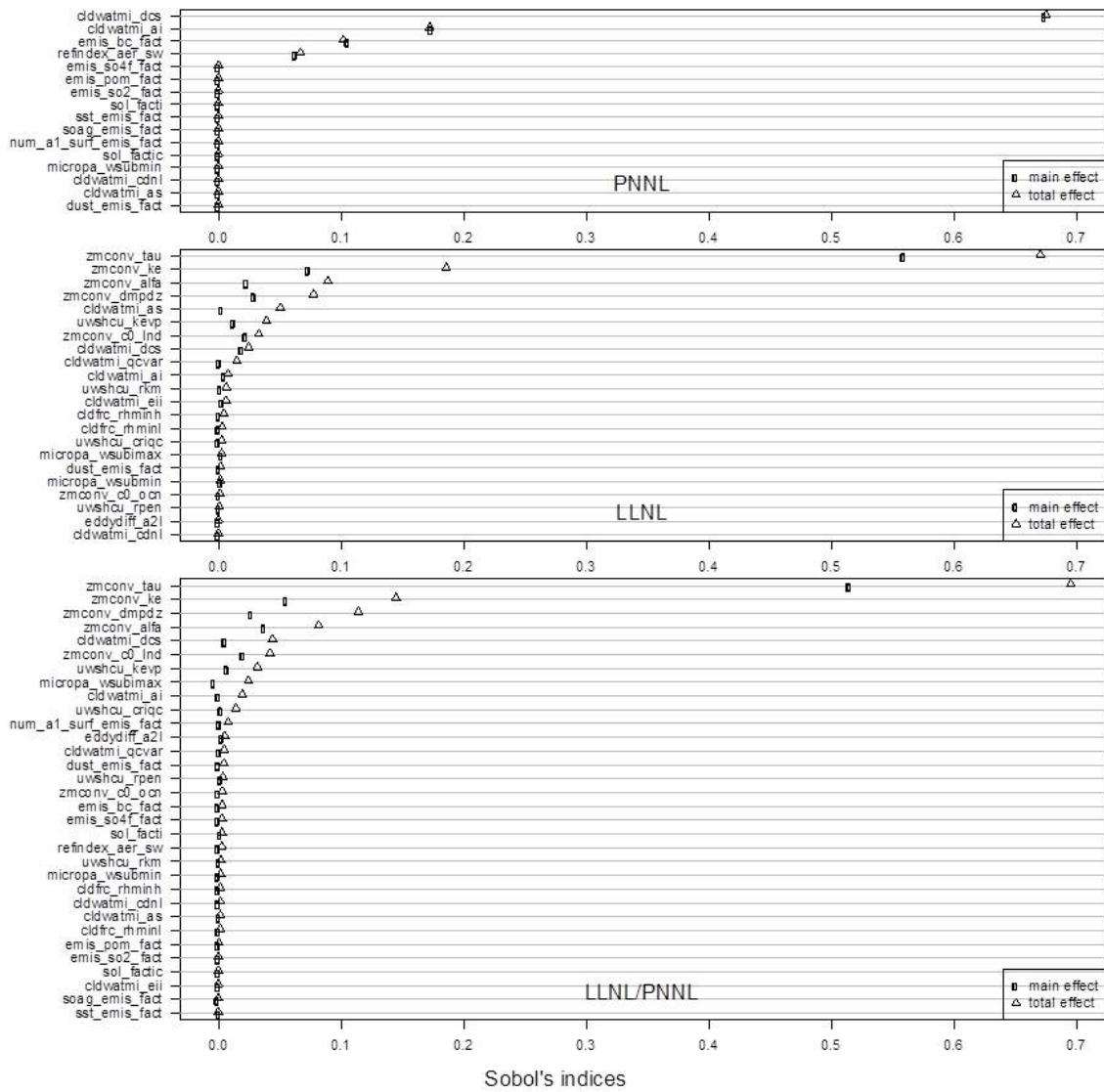
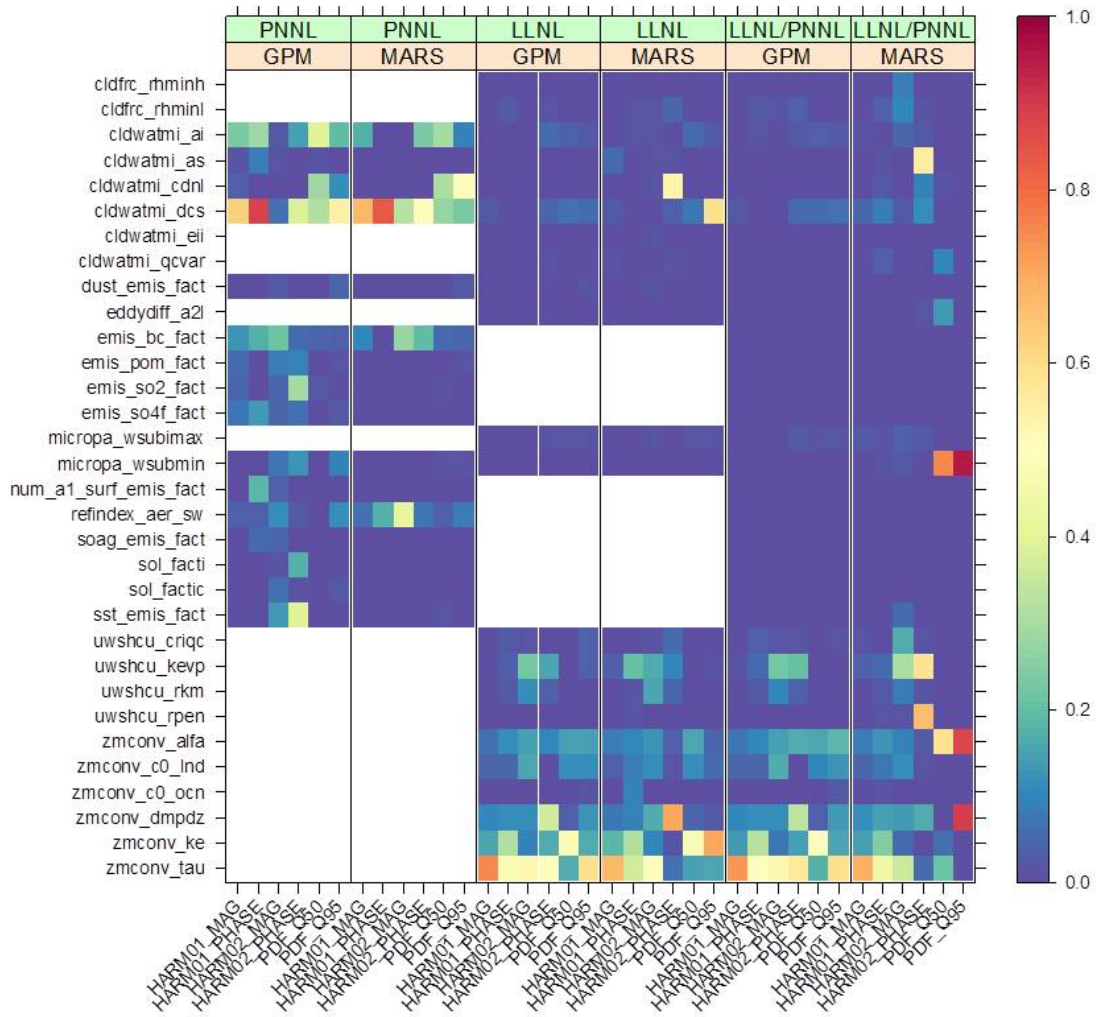


Figure 3.20. Sobol' sensitivity indices for the magnitude of the 1st harmonic in region SGP in season JJA using MARS surrogates trained on the PNNL data (top), the LLNL data (middle), and using both the LLNL and PNNL data (bottom).



Sobol's total index for multiple metrics in the SGP region in JJA

Figure 3.21. Sobol' sensitivity indices for metrics in region SGP in season JJA using GPMs.

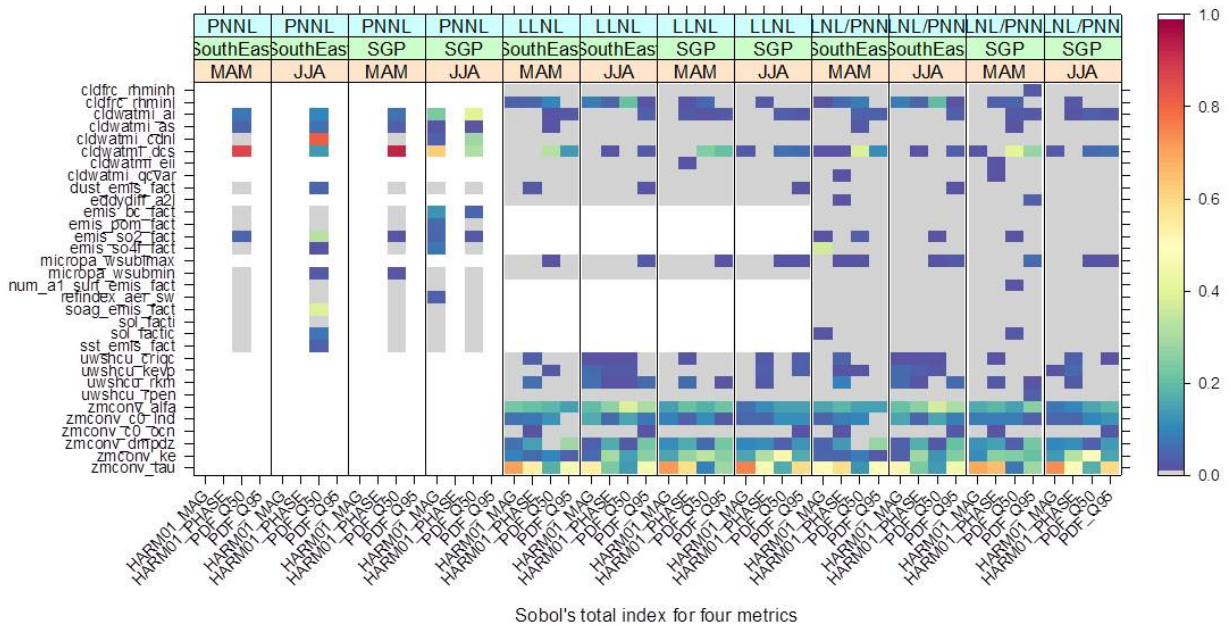


Figure 3.22. Sobol' sensitivity indices for four metrics in two regions and in two seasons using GPMs. The results have been filtered so that metrics where the Sobol' indices are less than 0.01 are colored grey and results are eliminated for GPMs with R-squared values less than 0.5

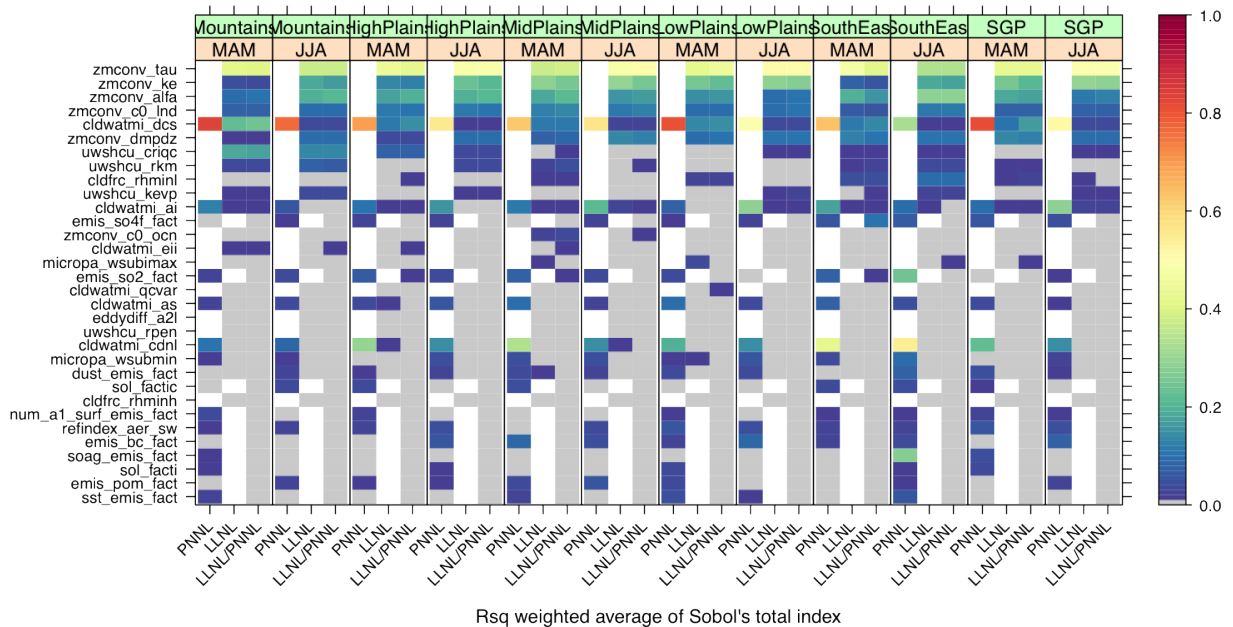


Figure 3.23. Sobol' total sensitivity indices averaged across metrics in each region/season for PNNL, LLNL, and joint LLNL/PNNL study. The metrics were averaged together using weights based on the GPM's R^2 .

Table of Average Sobol's Sensitivity Indices			
	PNNL	LLNL	LLNL/PNNL
zmconv_tau	NA	0.4431	0.4107
zmconv_alfa	NA	0.191	0.185
zmconv_ke	NA	0.1998	0.1781
zmconv_dmpdz	NA	0.1071	0.0992
cldwatmi_dcs	0.5789	0.0636	0.0857
zmconv_c0_ind	NA	0.0855	0.0825
cldfrc_rhminl	NA	0.0427	0.0444
emis_so4f_fact	0.0573	NA	0.0303
uwshcu_rkm	NA	0.0172	0.0165
uwshcu_kevp	NA	0.0136	0.0149
cldwatmi_ai	0.1612	0.0129	0.0135
uwshcu_criqc	NA	0.01	0.0105
micropa_wsubimax	NA	0.0057	0.0085
emis_so2_fact	0.0855	NA	0.0067
zmconv_c0_ocn	NA	0.0036	0.0053
cldwatmi_eii	NA	0.0035	0.0041
eddydiff_a2l	NA	0.0021	0.0039
cldwatmi_as	0.0419	0.0017	0.0038
sol_factic	0.0218	NA	0.0031
cldwatmi_qcvar	NA	0.0013	0.0029
uwshcu_rpen	NA	0.0013	0.0019
cldfrc_rhminh	NA	0.0008	0.0017
emis_bc_fact	0.0347	NA	0.0016
num_a1_surf_emis_fact	0.0205	NA	0.0014
soag_emis_fact	0.0852	NA	0.0013
refindex_aer_sw	0.0365	NA	0.0013
micropa_wsubmin	0.0415	0.0012	0.0011
sol_facti	0.0142	NA	0.001
cldwatmi_cdnl	0.3227	0.0005	0.0009
dust_emis_fact	0.0388	0.0028	0.0008
emis_pom_fact	0.0106	NA	0.0006
sst_emis_fact	0.0154	NA	0.0005

Figure 3.24. Averaged Sobol' indices across all regions and metrics, based on PNNL data, LLNL data, and joint data

Chapter 4

Conclusions

4.1 Joint sensitivity analyses

We aggregated the rankings from each of the three laboratories. This is shown in Figure 4.1. As mentioned, part of the goal of this exercise was to perform a downselection on the parameters that should be sampled in another CAM5 study at a higher resolution with a 1° study. The important parameters that should be analyzed in subsequent studies are highlighted in green. From the LLNL results, we focused on the averaged Sobol' indices from the LLNL data. From the PNNL studies, they provided ranks with a system of plusses and minuses, where a plus indicates a significant effect of that variable. Each parameter has five plusses or minuses, where each of the five represents a different metric. Finally, SNL reported a total fraction significant, which refers to the the fraction of the correlations and Sobol indices that were significant for a given parameter, i.e. the number for `zmconv_tau` is 0.75 indicating that 75% of the responses showed some significant dependence on `zmconv_tau`.

The results in Figure 4.1 show strong similarities of parameter rankings, although different methodologies were employed by each laboratory. This speaks to the robustness of the results and also to the fact that these methods were all global sensitivity analysis approaches.

The objective of this study was to identify a few parameters that are the most influential to the behavior of precipitation in CAM5, including the mean, extreme (95th percentile), and diurnal cycle. We analyzed the sensitivity of these precipitation metrics to cloud and atmospheric parameters, and we investigated how the sensitivity varies as a function of spatial scale, region, and season. The overall parameter rankings were very consistent. From the 32 parameters in our study, we were able to identify a downselect set of 14 influential parameters that we recommended be investigated in a set of 1° ensemble runs. These parameters include *tau*, *dcs*, *rhminl*, *c0_lnd*, *ke*, *alfa*, and *dmpdz*, among others. In addition to providing guidance on influential parameters for future studies relating to precipitation, this information may be used to guide the selection of parameters for calibration activities.

Param Name	Keep For 1 Degree	LLNL: Sobol	PNNL: Assessment	SNL: Signif. Fraction
dust_emis_fact	NO	0.0011	----+	0.0171
cldfrc_rhminh	NO	0.0010	----	0.0014
cldfrc_rhminl	YES	0.0214	--+++	0.0153
cldwatmi_ai	YES	0.0113	++++	0.1057
cldwatmi_as	MAYBE	0.0032	--+++	0.0297
cldwatmi_cdnl	YES	0.0018	++++	0.3071
cldwatmi_dcs	YES	0.0871	++++	0.2296
cldwatmi_eii	MAYBE	0.0065	----+	0.0153
cldwatmi_qcvar	NO	0.0031	----+	0.0083
eddydiff_a2l	NO	0.0025	----+	0.0069
micropa_wsibimax	NO	0.0058	----+	0.0028
micropa_wsubmin	MAYBE	0.0013	----+	0.0357
uwshcu_criqc	YES	0.0404	++++	0.1639
uwshcu_kevp	YES	0.0123	++++	0.0472
uwshcu_rkm	YES	0.0205	++++	0.0514
uwshcu_rpen	NO	0.0020	----+	0.0042
zmconv_alfa	YES	0.1749	++++	0.2194
zmconv_c0_lnd	YES	0.0983	++++	0.0792
zmconv_c0_ocn	YES	0.0061	++++	0.0097
zmconv_dmpdz	YES	0.0873	++++	0.1139
zmconv_ke	YES	0.1929	++++	0.1750
zmconv_tau	YES	0.4277	++++	0.7514
refindex_aer_sw	MAYBE	0.0010	---++	0.0575
sol_factic	MAYBE	0.0015	---++	0.0375
num_a1_surf_emis_fact	MAYBE	0.0012	---++	0.0300
soag_emis_fact	MAYBE	0.0008	---++	0.0250
sst_emis_fact	NO	0.0002	----	0.0275
sol_facti	MAYBE	0.0006	----+	0.0375
emis_so2_fact	YES	0.0057	++++	0.1125
emis_bc_fact	MAYBE	0.0010	---++	0.0275
emis_pom_fact	MAYBE	0.0005	---++	0.0175
emis_so4f_fact	MAYBE	0.0110	---++	0.0125

Figure 4.1. Ranking of CAM5 model parameters by different laboratories. Summary of downselect list: parameters highlighted in green should definitely be included in further 1° studies, those in red should be eliminated, and those in yellow perhaps included.

References

- [1] N. Cressie. *Statistics of Spatial Data*. John Wiley and Sons, New York, 1991.
- [2] J. H. Friedman. Multivariate adaptive regression splines. *Annals of Statistics*, 19(1):1–141, March 1991.
- [3] J. C. Helton and F. J. Davis. Latin hypercube sampling and the propagation of uncertainty in analyses of complex systems. *Reliability Engineering and System Safety*, 81(1):23–69, 2003.
- [4] R. L. Iman and M. J Shortencarier. A Fortran 77 program and user’s guide for the generation of latin hypercube samples for use with computer models. Technical Report NUREG/CR-3624, SAND83-2365, Sandia National Laboratories, Albuquerque, NM, 1984.
- [5] D. E. Knuth. *The Art of Computer Programming, Vol 2: Seminumerical algorithms. 3rd ed.* Addison-Wesley, Boston, 1997.
- [6] M. D. McKay, R. J. Beckman, and W. J. Conover. A comparison of three methods for selecting values of input variables in the analysis of output from a computer code. *Technometrics*, 21(2):239–245, 1979.
- [7] A. Saltelli. Sensitivity analysis: Could better methods be used? *Journal of Geophysical Research*, 104:3789–3793, 1999.
- [8] A. Saltelli, K. Chan, and E. M Scott. *Sensitivity Analysis*. Wiley, New York, 2000.
- [9] A. Saltelli, S. Tarantola, F. Campolongo, and M. Ratto. *Sensitivity Analysis in Practice: A Guide to Assessing Scientific Models*. John Wiley & Sons, 2004.

DISTRIBUTION:

- 1 Dorothy Koch
Program Manager, Climate and Environmental Sciences Division
SC-23, Germantown Building
U.S. Department of Energy
1000 Independence Avenue, SW
Washington, DC 20585-1290
- 1 David Bader
Lawrence Livermore National Laboratory
7000 East Avenue
Livermore, CA 94550
- 1 Stephen Klein
Lawrence Livermore National Laboratory
7000 East Avenue
Livermore, CA 94550
- 1 Gardar Johannesson
Lawrence Livermore National Laboratory
7000 East Avenue
Livermore, CA 94550
- 1 Donald Lucas
Lawrence Livermore National Laboratory
7000 East Avenue
Livermore, CA 94550
- 1 Yun Qian
Pacific Northwest National Laboratory
P.O. Box 999
Richland, WA 99352
- 1 William Collins
Lawrence Berkeley National Laboratory
1 Cyclotron Road Berkeley, CA 94720

- 1 MS 1318 J.R. Stewart, 01441
- 1 MS 1318 M.A. Taylor, 01442
- 1 MS 1318 L.P. Swiler, 01441
- 1 MS 1318 T.M. Wildey, 01441
- 1 MS 9051 B.J. Debusschere, 08351
- 1 MS 0899 RIM - Reports Management, 9532 (electronic copy)

